

¹ **Cross-scale interaction of host tree size and climate governs bark
2 beetle-induced tree mortality**

³ Michael J. Koontz^{1,2,3*}, Andrew M. Latimer^{1,2}, Leif A. Mortenson⁴, Christopher J. Fettig⁵, Malcolm P.
⁴ North^{1,2,6}

⁵ ¹Graduate Group in Ecology, University of California, Davis, CA, USA

⁶ ²Department of Plant Sciences, University of California, Davis, CA, USA

⁷ ³Earth Lab, University of Colorado-Boulder; Boulder, CO, USA

⁸ ⁴USDA Forest Service, Pacific Southwest Research Station, Placerville, CA, USA

⁹ ⁵USDA Forest Service, Pacific Southwest Research Station, Davis, CA, USA

¹⁰ ⁶USDA Forest Service, Pacific Southwest Research Station, Mammoth Lakes, CA, USA

¹¹ *Correspondence: michael.koontz@colorado.edu

¹² *Keywords:* *Dendroctonus brevicomis*, disturbance, drones, *Pinus ponderosa*, Sierra Nevada, structure from motion, forest structure, climate change-type drought, macroecology

¹⁴ *Abstract word count:*

¹⁵ *Overall .docx word count:*

¹⁶ *Main text word count:* (Intro: Results: ; Discussion:)

¹⁷ *Methods word count:* *Text boxes word count:* 0

¹⁸ Date report generated: May 01, 2020

¹⁹ **Abstract**

²⁰ The Californian hot drought of 2012 to 2015 created favorable conditions for unprecedented ponderosa pine
²¹ (*Pinus ponderosa*) mortality in the Sierra Nevada mountain range, largely attributable to the western pine
²² beetle (*Dendroctonus brevicomis*; WPB). Climate conditions can partially explain tree mortality patterns
²³ through their direct effect on tree vigor, but tree mortality rates can respond non-linearly to climate
²⁴ conditions when bark beetles interact with local forest characteristics while they colonize drought-stressed
²⁵ trees. Measuring broad-scale climate conditions simultaneously with local forest composition and structure–
²⁶ the spatial distribution and size of trees– will refine our understanding of how these variables interact, but
²⁷ is generally expensive and/or labor-intensive. We use drone surveys over 32 distinct sites along a 350-km
²⁸ latitudinal and 1000-m elevational gradient in western slope Sierra Nevada ponderosa pine/mixed-conifer
²⁹ forests and structure from motion (SfM) photogrammetry to segment and classify more than 450,000 trees

30 over 9 km² of forest with WPB-induced tree mortality. We validated the segmentation and classification
31 with data from 160 coincident field plots (each 0.041 ha in area) throughout the 32 sites, assuming that dead
32 trees were all ponderosa pine killed by WPB. We modeled the probability of ponderosa pine mortality as a
33 function of forest structure and composition and their interaction with site-level climatic water deficit (CWD),
34 accounting for spatial covariance using exact Gaussian processes. A greater local proportion of host trees
35 strongly increased the probability of host mortality, with greater host density amplifying this effect. Further,
36 we found a strong interaction between host size and CWD such that larger trees increased the probability of
37 host mortality at hot/dry sites, but smaller trees tended to drive mortality in cool/wet sites. Our results
38 demonstrate a variable response of WPB to local forest structure and composition across an environmental
39 gradient, which may help reconcile differences between observed ecosystem-wide tree mortality patterns and
40 predictions from models based on coarser-scale forest structure. Climate change adaptation strategies should
41 consider that future disturbance outcomes may depend on interactions between local forest structure and
42 broad-scale environmental gradients, with the potential for cross-scale interactions that challenge our current
43 understanding of forest insect dynamics.

44 Introduction

45 Bark beetles dealt the final blow to many of the nearly 150 million trees killed in the California hot drought of
46 2012 to 2015 and its aftermath (USDAFS 2019). A harbinger of climate change effects to come, record high
47 temperatures exacerbated the drought (Griffin and Anchukaitis 2014, Robeson 2015), which increased water
48 stress in trees (Asner et al. 2016, Brodrick and Asner 2017), making them more susceptible to colonization
49 by bark beetles (Fettig 2012, Kolb et al. 2016). Further, a century of fire suppression policy has enabled
50 forests to grow unchecked, which can also make them more vulnerable to bark beetles (Waring and Pitman
51 1985, Fettig 2012, Restaino et al. 2019). This combination of environmental conditions and forest structural
52 characteristics led to tree mortality events of unprecedented size across the state (Young et al. 2017, USDAFS
53 2017).

54 Tree mortality exhibited a strong latitudinal and elevational gradient (Asner et al. 2016, Young et al. 2017)
55 that can only be partially explained by coarse-scale measures of environmental conditions (i.e., historic
56 climatic water deficit; CWD) and current forest structure (i.e., current regional basal area) (Young et al.
57 2017). Progressive loss of canopy water content offers additional insight into tree vulnerability to mortality,
58 but cannot ultimately resolve which trees die in forests with bark beetles as a key mortality agent (Brodrick
59 and Asner 2017). Bark beetles respond to local forest characteristics in positive feedbacks that non-linearly
60 alter tree mortality dynamics against a background of environmental conditions that stress trees (Raffa et al.

61 2008, Boone et al. 2011). Thus, an explicit consideration of local forest structure and composition (Stephenson
62 et al. 2019, Fettig et al. 2019) as well as its cross-scale interaction with regional climate conditions (Senf
63 et al. 2017) can refine our understanding of tree mortality patterns from California's recent hot drought.
64 The challenge of simultaneously measuring the effects of both local-scale forest features (such as structure
65 and composition) and broad-scale environmental conditions (such as climatic water deficit; CWD) on forest
66 insect disturbance leaves their interaction effect relatively underexplored (Seidl et al. 2016, Senf et al. 2017,
67 Stephenson et al. 2019, Fettig et al. 2019).

68 The ponderosa pine/mixed-conifer forests in California's Sierra Nevada region are characterized by regular
69 bark beetle disturbances, primarily by the influence of western pine beetle (*Dendroctonus brevicomis*; WPB)
70 on its host ponderosa pine (*Pinus ponderosa*) (Fettig 2016). WPB is a primary bark beetle— its reproductive
71 success is contingent upon host tree mortality, which itself requires enough beetles to mass attack the host tree
72 and overwhelm its defenses (Raffa and Berryman 1983). This Allee effect creates a strong coupling between
73 beetle selection behavior of host trees and host tree susceptibility to colonization (Raffa and Berryman 1983,
74 Logan et al. 1998, Wallin and Raffa 2004). A key defense mechanism of conifers to bark beetle attack is to
75 flood beetle bore holes with resin, which physically expels colonizing beetles, can be toxic to the colonizers
76 and their fungi, and may interrupt beetle communication (Franceschi et al. 2005, Raffa et al. 2015). Under
77 normal conditions, weakened trees with compromised defenses are the most susceptible to colonization and
78 will be the main targets of primary bark beetles like WPB (Bentz et al. 2010, Boone et al. 2011, Raffa et al.
79 2015). Under severe water stress, many trees no longer have the resources available to mount a defense (Boone
80 et al. 2011, Kolb et al. 2016) and thus prolonged drought can often trigger increased bark beetle-induced
81 tree mortality as average tree vigor declines (Bentz et al. 2010) (though we note that the inciting factors
82 for increased tree mortality in other bark beetle systems, such as mountain pine beetle in lodgepole pine,
83 may be more related to temperature's effect on the beetle's physiology). As the local population density of
84 beetles increases due to successful reproduction within spatially-aggregated weakened trees, as might occur
85 during drought, mass attacks grow in size and become capable of overwhelming formidable tree defenses
86 such that even healthy trees may be susceptible to colonization and mortality (Bentz et al. 2010, Boone et
87 al. 2011, Raffa et al. 2015). Thus, water stress can be a key determinant of whether individual trees are
88 susceptible to bark beetles under many conditions, and this environmental condition may interact with beetle
89 population dynamics to drive tree susceptibility under extreme conditions (Bentz et al. 2010, Boone et al.
90 2011, Stephenson et al. 2019).

91 WPB activity is strongly influenced by forest structure— the spatial distribution and size of trees— and tree
92 species composition. Taking forest structure alone, high-density forests are more prone to bark beetle-induced

tree mortality (Fettig 2012) which may arise as greater competition for water resources amongst crowded trees and thus average tree resistance is lower (Hayes et al. 2009), or because smaller gaps between trees protect pheromone plumes from dissipation by the wind and thus enhance intraspecific beetle communication (Thistle et al. 2004). Tree size is another aspect of forest structure that affects bark beetle host selection behavior with smaller trees tending to have lower capacity for resisting attack, and larger trees being more desirable targets on account of their thicker phloem providing greater nutritional content (Miller and Keen 1960, Chubaty et al. 2009, Boone et al. 2011, Graf et al. 2012). Throughout an outbreak, some bark beetle species will collectively “switch” the preferred size of tree to attack in order to navigate the trade-off between host susceptibility and host quality (Geiszler and Gara 1978, Klein et al. 1978, Mitchell and Preisler 1991, Preisler 1993, Wallin and Raffa 2004). Taking forest composition alone, WPB activity in the Sierra Nevada mountain range of California is necessarily tied to the regional distribution of its exclusive host, ponderosa pine (Fettig 2016). Colonization by primary bark beetles can also depend on the relative frequencies of tree species in a more local area, akin to reduced oligophagous insect herbivory in forests comprising taxonomically-distinct tree species compared to monocultures (Jactel and Brockerhoff 2007). The interaction between forest structure and composition also drives WPB activity. For instance, high-density forests with high host availability may experience greater beetle-induced tree mortality because dispersal distances between potential host trees are shorter reducing predation of adults searching for hosts and facilitating higher rates of colonization (Miller and Keen 1960, Berryman 1982, Fettig et al. 2007) or because high host availability reduces the chance of individual beetles wasting their limited resources flying to and landing on a non-host tree (Moeck et al. 1981, Evenden et al. 2014). Stand-scale measures of forest structure and composition thus paint a fundamentally limited picture of the mechanisms by which these forest characteristics affect bark beetle disturbance, but finer-grain information explicitly recognizing tree size, tree species, and local tree density should more appropriately capture the ecological processes underlying insect-induced tree mortality (Geiszler and Gara 1978, Mitchell and Preisler 1991, Preisler 1993, Kaiser et al. 2013). Additionally, considering the effects of local forest structure and composition with the effects of environmental conditions may help refine our understanding of tree mortality patterns in widespread events such as during the recent California hot drought.

The vast spatial extent of tree mortality in the 2012 to 2015 California hot drought challenges our ability to simultaneously consider how broad-scale environmental conditions may interact with local forest structure and composition to affect the dynamic between bark beetle selection and colonization of host trees, and host tree susceptibility to attack (Anderegg et al. 2015, Stephenson et al. 2019). Measuring local forest structure generally requires expensive instrumentation (Kane et al. 2014, Asner et al. 2016) or labor-intensive field

125 surveys (Larson and Churchill 2012, Stephenson et al. 2019, Fettig et al. 2019), which constrains survey
126 extent and frequency. Small, unhumanned aerial systems (sUAS) enable relatively fast and cheap remote
127 imaging over hundreds of hectares of forest, which can be used to measure complex forest structure and
128 composition at the individual tree scale with Structure from Motion (SfM) photogrammetry (Morris et al.
129 2017, Shiklomanov et al. 2019). The ultra-high resolution of sUAS-derived measurements as well as the
130 ability to incorporate vegetation reflectance can help overcome challenges in species classification and dead
131 tree detection inherent in other remote sensing methods, such as airborne LiDAR (Jeronimo et al. 2019).
132 Distributing such surveys across an environmental gradient can overcome the data acquisition challenge
133 inherent in investigating phenomena with both a strong local- and a strong broad-scale component.

134 We used sUAS-derived remote sensing images over a network of 32 sites in Sierra Nevada ponderosa pine/mixed-
135 conifer forests spanning 1000 m of elevation and 350 km of latitude (see Fettig et al. 2019) and covering a
136 total of 9 km² to ask how broad-scale environmental conditions interacted with local forest structure and
137 composition to shape patterns of tree mortality rates during the cumulative tree mortality event of 2012 to
138 2018. We asked:

- 139 1. How does the proportion of host trees in a local area and average host tree size affect WPB-induced
140 tree mortality?
- 141 2. How does the density of all tree species (hereafter “overall density”) affect WPB-induced tree mortality?
- 142 3. How does environmentally-driven tree moisture stress affect WPB-induced tree mortality?
- 143 4. Do the effects of forest structure, forest composition, and environmental condition interact to influence
144 WPB-induced tree mortality?

145 Methods

146 Study system

147 We built our study coincident with 160 vegetation/forest insect monitoring plots at 32 sites established
148 between 2016 and 2017 by Fettig et al. (2019) (Figure 1). The study sites were chosen to reflect typical
149 west-side Sierra Nevada yellow pine/mixed-conifer forests and were dominated by ponderosa pine (Fettig
150 et al. 2019). Plots were located in WPB-attacked, yellow pine/mixed-conifer forests across the Eldorado,
151 Stanislaus, Sierra and Sequoia National Forests and were stratified by elevation (914-1219 m, 1219-1524
152 m, 1524-1829 m above sea level). In the Sequoia National Forest, the southernmost National Forest in our
153 study, plots were stratified with the lowest elevation band of 1219-1524 m and extended to an upper elevation
154 band of 1829-2134 m to capture a more similar forest community composition as at the more northern

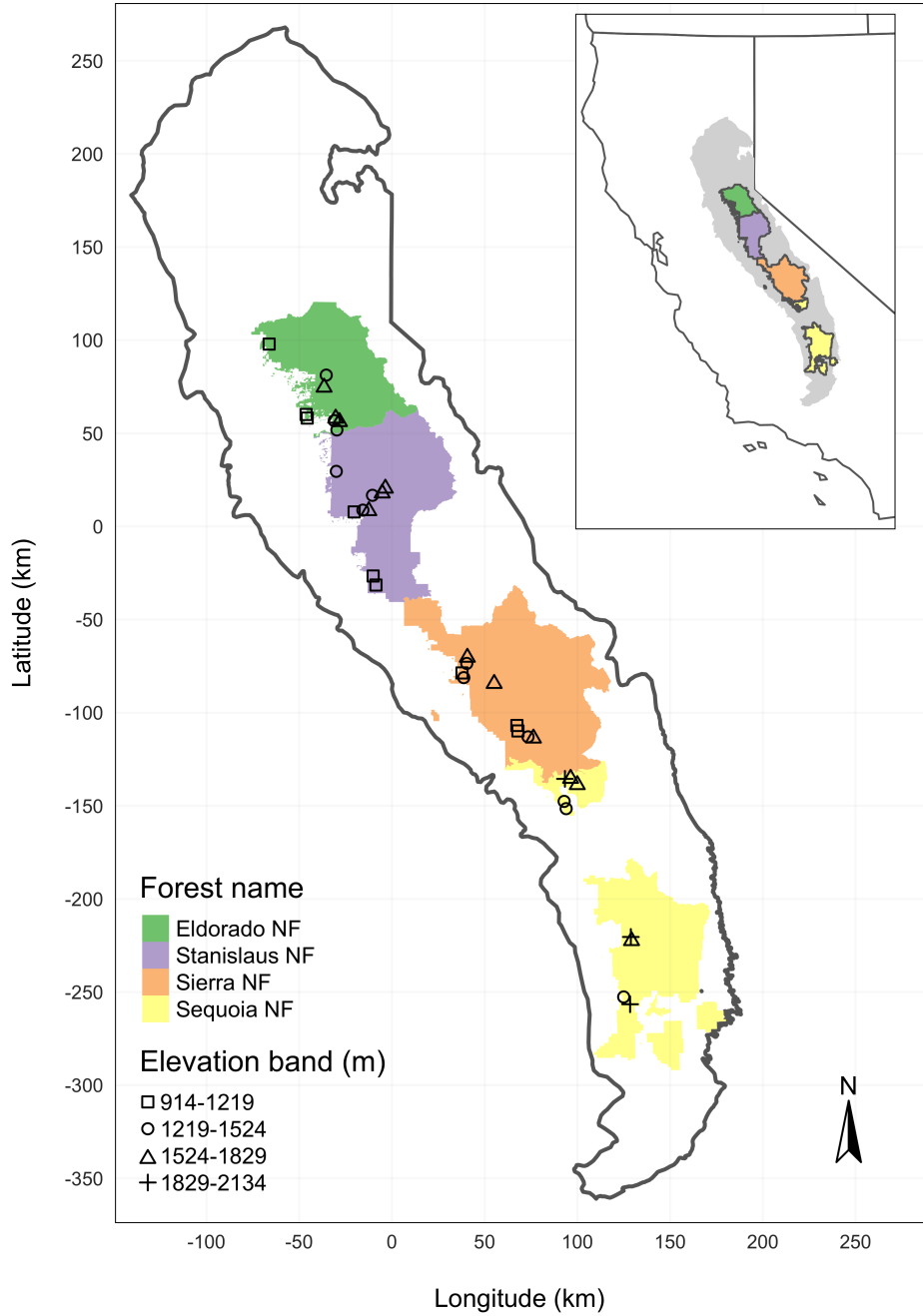


Figure 1: The network of field plots spanned a 350-km latitudinal gradient from the Eldorado National Forest in the north to the Sequoia National Forest in the south. Plots were stratified by three elevation bands in each forest, with the plots in the Sequoia National Forest (the southern-most National Forest) occupying elevation bands 305 m above the three bands in the other National Forests in order to capture a similar community composition.

155 National Forests. The sites have variable forest structure and plot locations were selected in areas with >35%
156 ponderosa pine basal area and >10% ponderosa pine mortality. At each site, five 0.041 ha circular plots
157 were installed along transects with 80 to 200m between plots. In the field, Fettig et al. (2019) mapped all
158 stem locations relative to the center of each plot using azimuth/distance measurements. Tree identity to
159 species, tree height, and diameter at breast height (DBH) were recorded if DBH was greater than 6.35cm.
160 Year of mortality was estimated based on needle color and retention if it occurred prior to plot establishment,
161 and was directly observed thereafter during annual site visits. A small section of bark (approximately 625
162 cm²) on both north and south aspects was removed from dead trees to determine if bark beetle galleries
163 were present. The shape, distribution, and orientation of galleries are commonly used to distinguish among
164 bark beetle species (Fettig 2016). In some cases, deceased bark beetles were present beneath the bark to
165 supplement identifications based on gallery formation. During the spring and early summer of 2018, all field
166 plots were revisited to assess whether dead trees had fallen (Fettig et al. 2019).

167 In the typical life cycle of WPBs, females initiate host colonization by tunneling through the outer bark and
168 into the phloem and outer xylem where they rupture resin canals.

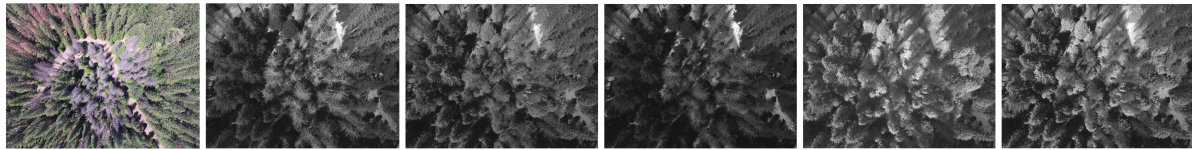
169 As a result, oleoresin exudes and collects on the bark surface, as is commonly observed with other bark beetle
170 species. During the early stages of attack, females release an aggregation pheromone component which, in
171 combination with host monoterpenes released from pitch tubes, is attractive to conspecifics (Bedard et al.
172 1969). An antiaggregation pheromone component is produced during latter stages of host colonization by
173 several pathways, and is thought to reduce intraspecific competition by altering adult behavior to minimize
174 overcrowding of developing brood within the host (Byers and Wood 1980). Volatiles from several nonhosts
175 sympatric with ponderosa pine have been demonstrated to inhibit attraction of WPB to its aggregation
176 pheromones (Shepherd et al. 2007, Fettig and Hilszczański 2015). In California, WPB generally has 2-3
177 generations in a single year and can often out-compete other primary bark beetles such as the mountain pine
178 beetle (*Dendroctonus ponderosae*), in ponderosa pines, especially in larger trees (Miller and Keen 1960).

179 **Aerial data collection and processing**

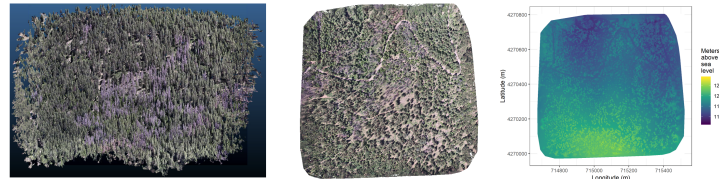
180 Nadir-facing imagery was captured using a gimbal-stabilized DJI Zenmuse X3 broad-band red/green/blue
181 (RGB) camera (DJI 2015a) and a fixed-mounted Micasense Rededge3 multispectral camera with five narrow
182 bands (Micasense 2015) on a DJI Matrice 100 aircraft (DJI 2015b). Imagery was captured from both cameras
183 along preprogrammed aerial transects over ~40 hectares surrounding each of the 32 sites (each of these
184 containing five field plots) and was processed in a series of steps to yield local forest structure and composition
185 data suitable for our statistical analyses. All images were captured in 2018 during a 3-month period between

186 early April and early July, and thus our work represents a postmortem investigation into the drivers of
187 cumulative tree mortality through the course of the hot drought. Following the call by Wyngaard et al.
188 (2019), we establish “data product levels” to reflect the image processing pipeline from raw imagery (Level 0)
189 to calibrated, fine-scale forest structure and composition information on regular grids (Level 4), with each
190 new data level derived from levels below it. Here, we outline the steps in the processing and calibration
191 pipeline visualized in Figure 2, and include additional details in the Supplemental Information.

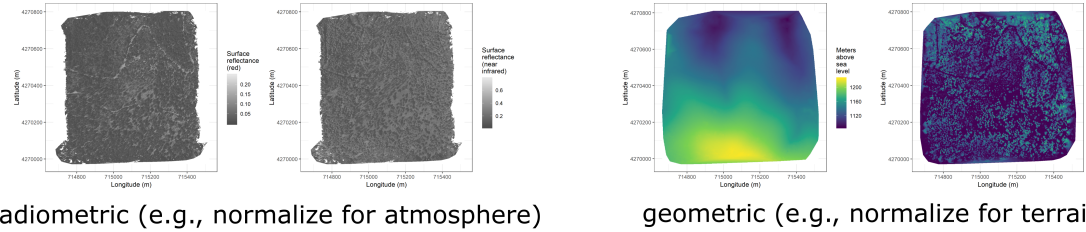
Level 0: raw data from sensors



Level 1: basic outputs from photogrammetric processing



Level 2: corrected outputs from photogrammetric processing

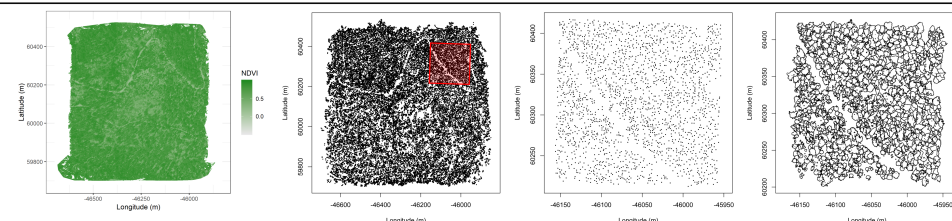


radiometric (e.g., normalize for atmosphere)

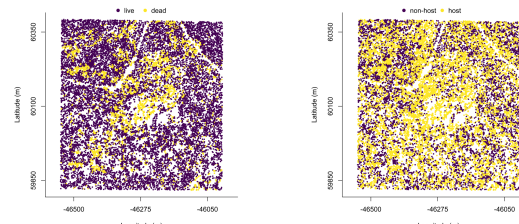
geometric (e.g., normalize for terrain)

Level 3: domain-specific information extraction

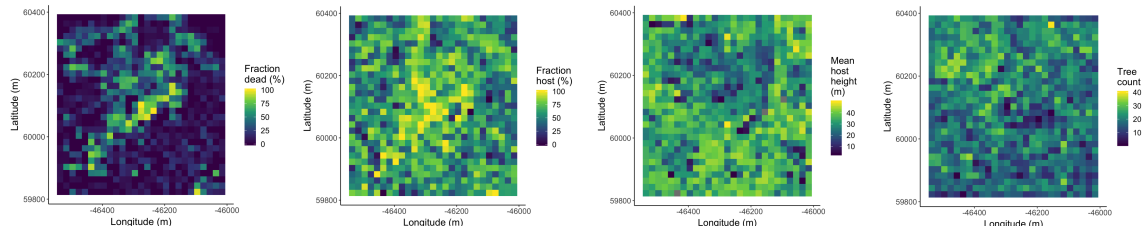
L3a
spectral
OR
geometric



L3b
spectral
AND
geometric



Level 4: aggregations to regular grids



193 Figure 2. Schematic of the data processing workflow for a single site with each new data product level derived
194 from data at lower levels.

195 Level 0 represents raw data from the sensors. From left to right: example broad-band RGB photo from
196 DJI Zenmuse X3 camera, example blue photo from Rededge3 (centered on 475nm), example green photo
197 from Rededge3 (centered on 560nm), example red photo from Rededge3 (centered on 668nm), example near
198 infrared photo from Rededge3 (centered on 840nm), and example red edge photo from Rededge3 (centered on
199 717nm).

200 Level 1 represents basic outputs from the photogrammetric workflow, in this case implemented with
201 Pix4Dmapper. From left to right: a dense point cloud visualized in CloudCompare (<https://www.danielgm.net/cc/>), an orthophoto generated from the RGB camera, and a digital surface model representing the
202 altitude above sea level (ground height + vegetation height) for every cell.

204 Level 2 represents outputs from photogrammetric processing that have been corrected radiometrically or
205 geometrically. From left to right: a radiometrically-corrected surface reflectance map of the red narrow band
206 from the Rededge3 camera, a radiometrically-corrected surface reflectance map of the near infrared narrow
207 band from the Rededge3 camera, a rasterized version of the digital terrain model derived by a geometric
208 correction of the dense point cloud, and a canopy height model derived by subtracting the terrain height
209 from the digital surface model.

210 Level 3 represents domain-specific information extraction from Level 2 products and is divided into two
211 sub-levels. Level 3a products are derived using only spectral or only geometric data. From left to right: a
212 reflectance map of Normalized Difference Vegetation Index (NDVI; Rouse et al. (1973)) derived using the red
213 and near infrared Level 2 reflectance products, a map of points representing detected trees from the canopy
214 height model with a red polygon highlighting the area presented in more detail for the next two images, a
215 close-up of points representing detected trees, and a close-up of polygons representing segmented tree crowns.
216 Level 3b products are derived using both spectral and geometric data. From left to right: a map of the point
217 locations of detected trees that have been classified as alive or dead based on the pixel values within each
218 segmented tree crown and a map of the point locations of detected trees classified to WPB host/non-host
219 using the same spectral information. Note that our study relies on the generation of Level 3a products in
220 order to combine them and create Level 3b products, but this need not be the case. For instance, deep
221 learning/neural net methods may be able to use both the spectral and geometric information from Level 2
222 simultaneously to locate and classify trees in a scene and directly generate Level 3b products without a need
223 to first generate the Level 3a products shown in this schematic (Weinstein et al. 2019, dos Santos et al. 2019).

224 Level 4 represents aggregations of Level 3 products to regular grids which might better reflect the grain size
225 of the data for which we have the best calibration and thus the most confidence or which might provide
226 new information not possible at an individual-tree level (e.g., average distance between trees in a small
227 neighborhood). From left to right: aggregation of live/dead classified trees as fraction of dead trees in a 20 x
228 20-m cell, aggregation of host/non-host classified trees as fraction of hosts in a 20 x 20-m cell, aggregation of
229 mean host height in a 20 x 20-m cell, and aggregation of tree count (including all species), in a 20 x 20-m
230 cell. In our case, the 20 x 20-m aggregation produces a grid cell with an area of 400 m², which most closely
231 matches the 404-m² area of the ground-based vegetation plots whose data we used in an aggregated form to
232 calibrate our derivation of Level 3 products.

233 **Level 0: Raw data from sensors**

234 Raw data comprised approximately 1900 images per camera lens (one broad-band RGB lens and five narrow-
235 band multispectral lenses) for each of the 32 sites (Figure 2; Level 0). Prior to the aerial survey, two strips of
236 bright orange drop cloth (~100 x 15 cm) were positioned as an “X” over the permanent monuments marking
237 the center of the 5 field plots from Fettig et al. (2019) (see Supplemental Information).

238 We preprogrammed north-south aerial transects using Map Pilot for DJI on iOS flight software (Drones-
239 MadeEasy 2018) at an altitude of 120 m above ground level (with “ground” defined using a 1-arc-second
240 digital elevation model (Farr et al. 2007)). The resulting ground sampling distance was approximately 5
241 cm/px for the Zenmuse X3 RGB camera and approximately 8 cm/px for the Rededge3 multispectral camera.
242 We used 91.6% image overlap (both forward and side) at the ground for the Zenmuse X3 RGB camera and
243 83.9% overlap (forward and side) for the Rededge3 multispectral camera.

244 **Level 1: Basic outputs from photogrammetric processing**

245 We used SfM photogrammetry implemented in Pix4Dmapper Cloud (www.pix4d.com) to generate dense point
246 clouds (Figure 2; Level 1, left), orthophotos (Figure 2; Level 1, center), and digital surface models (Figure 2;
247 Level 1, right) for each field site (Frey et al. 2018). For 29 sites, we processed the Rededge3 multispectral
248 imagery alone to generate these products. For three sites, we processed the RGB and the multispectral
249 imagery together to enhance the point density of the dense point cloud. All SfM projects resulted in a single
250 processing “block,” indicating that all images in the project were optimized and processed together. The
251 dense point cloud represents x, y, and z coordinates as well as the color of millions of points per site. The
252 orthophoto represents a radiometrically uncalibrated, top-down view of the survey site that preserves the
253 relative x-y positions of objects in the scene. The digital surface model is a rasterized version of the dense

254 point cloud that shows the altitude above sea level for each pixel in the scene at the ground sampling distance
255 of the camera that generated the Level 0 data.

256 **Level 2: Corrected outputs from photogrammetric processing**

257 **Radiometric corrections**

258 A radiometrically-corrected reflectance map (Figure 2; Level 2, left two figures; i.e., a corrected version of the
259 Level 1 orthophoto) was generated using the Pix4D software by incorporating incoming light conditions for
260 each narrow band of the Rededge3 camera (captured simultaneously with the Rededge3 camera using an
261 integrated downwelling light sensor) as well as a pre-flight image of a calibration panel of known reflectance
262 (see Supplemental Information for camera and calibration panel details).

263 **Geometric corrections**

264 We implemented a geometric correction to the Level 1 dense point cloud and digital surface model by
265 normalizing these data for the terrain underneath the vegetation. We generated the digital terrain model
266 representing the ground underneath the vegetation at 1-m resolution (Figure 2; Level 2, third image) by
267 classifying each survey area’s dense point cloud into “ground” and “non-ground” points using a cloth simulation
268 filter algorithm (Zhang et al. 2016) implemented in the `lidR` (Roussel et al. 2019) package and rasterizing
269 the ground points using the `raster` package (Hijmans et al. 2019). We generated a canopy height model
270 (Figure 2; Level 2, fourth image) by subtracting the digital terrain model from the digital surface model.

271 **Level 3: Domain-specific information extraction**

272 **Level 3a: Data derived from spectral OR geometric Level 2 product**

273 Using just the spectral information from the radiometrically-corrected reflectance maps, we calculated several
274 vegetation indices including the normalized difference vegetation index (NDVI; Rouse et al. (1973); Figure
275 2; Level 3a, first image), the normalized difference red edge (NDRE; Gitelson and Merzlyak (1994)), the
276 red-green index (RGI; Coops et al. (2006)), the red edge chlorophyll index ($CI_{red\ edge}$; Clevers and Gitelson
277 (2013)), and the green chlorophyll index (CI_{green} ; Clevers and Gitelson (2013)).

Table 1: Algorithm name, number of parameter sets tested for each algorithm, and references.

Algorithm	Parameter sets tested	Reference(s)
li2012	131	Li et al. (2012); Jakubowski et al. (2013); Shin et al. (2018)

Algorithm	Parameter sets tested	Reference(s)
lmfx	30	Roussel (2019)
localMaxima	6	Roussel et al. (2019)
multichm	1	Eysn et al. (2015)
ptrees	3	Vega et al. (2014)
vwf	3	Plowright (2018)
watershed	3	Pau et al. (2010)

Using just the geometric information from the canopy height model or terrain-normalized dense point cloud, we generated maps of detected trees (Figure 2; Level 3a, second and third images) by testing a total of 7 automatic tree detection algorithms and a total of 177 parameter sets (Table 1). We used the field plot data to assess each tree detection algorithm/parameter set by converting the distance-from-center and azimuth measurements of the trees in the field plots to x-y positions relative to the field plot centers distinguishable in the Level 2 reflectance maps as the orange fabric X's that we laid out prior to each flight. In the reflectance maps, we located 110 out of 160 field plot centers while some plot centers were obscured due to dense interlocking tree crowns or because a plot center was located directly under a single tree crown. For each of the 110 field plots with identifiable plot centers— the “validation field plots”, we calculated 7 forest structure metrics using the ground data collected by Fettig et al. (2019): total number of trees, number of trees greater than 15 m in height, mean height of trees, 25th percentile tree height, 75th percentile tree height, mean distance to nearest tree neighbor, and mean distance to second nearest neighbor. For each tree detection algorithm and parameter set described above, we calculated the same set of 7 structure metrics within the footprint of the validation field plots. We calculated the Pearson’s correlation and root mean square error (RMSE) between the ground data and the aerial data for each of the 7 structure metrics for each of the 177 automatic tree detection algorithms/parameter sets. For each algorithm and parameter set, we calculated its performance relative to other algorithms as whether its Pearson’s correlation was within 5% of the highest Pearson’s correlation as well as whether its RMSE was within 5% of the lowest RMSE. We summed the number of forest structure metrics for which it reached these 5% thresholds for each algorithm/parameter set. For automatically detecting trees across the whole study, we selected the algorithm/parameter set that performed well across the most number of forest metrics (see Results).

We delineated individual tree crowns (Figure 2; Level 3a, fourth image) with a marker controlled watershed segmentation algorithm (Meyer and Beucher 1990) implemented in the **ForestTools** package (Plowright

301 2018) using the detected treetops as markers. If the automatic segmentation algorithm failed to generate
302 a crown segment for a detected tree (e.g., often snags with a very small crown footprint), a circular crown
303 was generated with a radius of 0.5 m. If the segmentation generated multiple polygons for a single detected
304 tree, only the polygon containing the detected tree was retained. Because image overlap decreases near the
305 edges of the overall flight path and reduces the quality of the SfM processing in those areas, we excluded
306 segmented crowns within 35 m of the edge of the survey area. Given the narrower field of view of the
307 Rededge3 multispectral camera versus the X3 RGB camera whose optical parameters were used to define the
308 ~40 hectare survey area around each site, as well as the 35 m additional buffering, the survey area at each
309 site was ~30 ha (see Supplemental Information).

310 **Level 3b: Data derived from spectral AND geometric information**

311 We overlaid the segmented crowns on the reflectance maps from 20 sites spanning the latitudinal and elevation
312 gradient in the study. Using QGIS (<https://qgis.org/en/site/>), we hand classified 564 trees as live/dead
313 (Figure 3) and as one of 5 dominant species in the study area (ponderosa pine, *Pinus lambertiana*, *Abies*
314 *concolor*, *Calocedrus decurrens*, or *Quercus kelloggii*) using the mapped ground data as a guide. Each tree was
315 further classified as “host” for ponderosa pine or “non-host” for all other species (Fettig 2016). We extracted
316 all the pixel values within each segmented crown polygon from the five, Level 2 orthorectified reflectance
317 maps (one per narrow band on the Rededge3 camera) as well as from the five, Level 3a vegetation index
318 maps using the **velox** package (Hunziker 2017). For each crown polygon, we calculated the mean value of the
319 extracted Level 2 and Level 3a pixels and used them as ten independent variables in a five-fold cross validated
320 boosted logistic regression model to predict whether the hand classified trees were alive or dead. For just the
321 living trees, we similarly used all 10 mean reflectance values per crown polygon to predict tree species using a
322 five-fold cross validated regularized discriminant analysis. The boosted logistic regression and regularized
323 discriminant analysis were implemented using the **caret** package in R (Kuhn 2008). We used these models to
324 classify all tree crowns in the data set as alive or dead (Figure 2; Level 3b, first image) as well as the species
325 of living trees (Figure 2; Level 3b, second image). Finally, we estimated the basal area of each tree from their
326 photogrammetry-derived height using species-specific simple linear regressions of the relationship between
327 height and diameter at breast height as measured in the coincident field plots from Fettig et al. (2019).

328 **Level 4: Aggregations to regular grids**

329 We rasterized the forest structure and composition data at a spatial resolution similar to that of the field
330 plots to better match the grain size at which we validated the automatic tree detection algorithms. In each
331 raster cell, we calculated: number of dead trees, number of ponderosa pine trees, total number of trees, and

332 mean height of ponderosa pine trees. The values of these variables in each grid cell and derivatives from
333 them were used for visualization and modeling. Here, we show the fraction of dead trees per cell (Figure 2;
334 Level 4, first image), the fraction of host trees per cell (Figure 2; Level 4, second image), the mean height of
335 ponderosa pine trees in each cell (Figure 2; Level 4, third image), and the total count of trees per cell (Figure
336 2; Level 4, fourth image).

337 Note on assumptions about dead trees

338 For the purposes of this study, we assumed that all dead trees were ponderosa pine and thus hosts colonized
339 by WPB. This is a reasonably good assumption for our study area; for example, Fettig et al. (2019) found
340 that 73.4% of dead trees in their coincident field plots were ponderosa pine. Mortality was concentrated in
341 the larger-diameter classes and attributed primarily to WPB (see Figure 5 of Fettig et al. 2019). The species
342 contributing to the next highest proportion of dead trees was incense cedar which represented 18.72% of the
343 dead trees in the field plots. While the detected mortality is most likely to be ponderosa pine killed by WPB,
344 it is critical to interpret our results with these limitations in mind.

345 Environmental data

346 We used CWD (Stephenson 1998) from the 1981-2010 mean value of the basin characterization model (Flint
347 et al. 2013) as an integrated measure of temperature and moisture conditions for each of the 32 sites. Higher
348 values of CWD correspond to hotter, drier conditions and lower values correspond to cooler, wetter conditions.
349 CWD has been shown to correlate well with broad patterns of tree mortality in the Sierra Nevada (Young et
350 al. 2017) as well as bark beetle-induced tree mortality (Millar et al. 2012). The forests along the entire CWD
351 gradient used in this study experienced exceptional hot drought between 2012 to 2015 with a severity of at
352 least a 1,200-year event, and perhaps more severe than a 10,000-year event (Griffin and Anchukaitis 2014,
353 Robeson 2015). We converted the CWD value for each site into a z-score representing that site's deviation
354 from the mean CWD across the climatic range of Sierra Nevada ponderosa pine as determined from 179
355 herbarium records described in Baldwin et al. (2017). Thus, a CWD z-score of 1 would indicate that the
356 CWD at that site is one standard deviation hotter/drier than the mean CWD across all geolocated herbarium
357 records for ponderosa pine in the Sierra Nevada.

358 Statistical model

359 We used a generalized linear model with a zero-inflated binomial response and a logit link to predict the
360 probability of ponderosa pine mortality within each 20 x 20-m cell using the total number of ponderosa
361 pine trees in each cell as the number of trials, and the number of dead trees in each cell as the number of

362 “successes”. As covariates, we used the proportion of trees that are WPB hosts (i.e., ponderosa pine) in each
 363 cell, the mean height of ponderosa pine trees in each cell, the count of trees of all species (overall density) in
 364 each cell, and the site-level CWD using Eq. 1. Note that the two-way interaction between the overall density
 365 and the proportion of trees that are hosts is directly proportional to the number of ponderosa pine trees in
 366 the cell. We centered and scaled all predictor values, and used weakly-regularizing default priors from the
 367 `brms` package (Bürkner 2017). To measure and account for spatial autocorrelation underlying ponderosa pine
 368 mortality, we subsampled the data at each site to a random selection of 200, 20 x 20-m cells representing
 369 approximately 27.5% of the surveyed area. Additionally with these subsampled data, we included a separate
 370 exact Gaussian process term per site of the noncentered/nonscaled interaction between the x- and y-position
 371 of each cell using the `gp()` function in the `brms` package (Bürkner 2017). The Gaussian process estimates the
 372 spatial covariance in the response variable (log-odds of ponderosa pine mortality) jointly with the effects of
 373 the other covariates.

$$\begin{aligned}
 y_{i,j} &\sim \begin{cases} 0, & p \\ Binom(n_i, \pi_i), & 1 - p \end{cases} \\
 logit(\pi_i) &= \beta_0 + \\
 &\beta_1 X_{cwd,j} + \beta_2 X_{propHost,i} + \beta_3 X_{PipoHeight,i} + \\
 &\beta_4 X_{overallDensity,i} + \beta_5 X_{overallBA,i} + \\
 &\beta_6 X_{cwd,j} X_{PipoHeight,i} + \beta_7 X_{cwd,j} X_{propHost,i} + \\
 &\beta_8 X_{cwd,j} X_{overallDensity,i} + \beta_9 X_{cwd,j} X_{overallBA,i} + \\
 &\beta_{10} X_{propHost,i} X_{PipoHeight,i} + \beta_{11} X_{propHost,i} X_{overallDensity,i} + \\
 &\beta_{12} X_{cwd,j} X_{propHost,i} X_{PipoHeight,i} + \\
 &\mathcal{GP}_j(x_i, y_i)
 \end{aligned}$$

374 Where y_i is the number of dead trees in cell i , n_i is the sum of the dead trees (assumed to be ponderosa pine)
 375 and live ponderosa pine trees in cell i , π_i is the probability of ponderosa pine tree mortality in cell i , p is the
 376 probability of there being zero dead trees in a cell arising as a result of an independent, unmodeled process,
 377 $X_{cwd,j}$ is the z-score of CWD for site j , $X_{propHost,i}$ is the scaled proportion of trees that are ponderosa pine
 378 in cell i , $X_{PipoHeight,i}$ is the scaled mean height of ponderosa pine trees in cell i , $X_{overallDensity,i}$ is the scaled
 379 density of all trees in cell i , $X_{overallBA,i}$ is the scaled basal area of all trees in cell i , x_i and y_i are the x- and
 380 y- coordinates of the centroid of the cell in an EPSG3310 coordinate reference system, and \mathcal{GP}_j represents

381 the exact Gaussian process describing the spatial covariance between cells at site j .
382 We fit this model using the `brms` package (Bürkner 2017) which implements the No U-Turn Sampler extension
383 to the Hamiltonian Monte Carlo algorithm (Hoffman and Gelman 2014) in the Stan programming language
384 (Carpenter et al. 2017). We used 4 chains with 4000 iterations each (2000 warmup, 2000 samples), and
385 confirmed chain convergence by ensuring all `Rhat` values were less than 1.1 (Brooks and Gelman 1998) and
386 that the bulk and tail effective sample sizes (ESS) for each estimated parameter were greater than 100 times
387 the number of chains (i.e., greater than 400 in our case). We used posterior predictive checks to visually
388 confirm model performance by overlaying the density curves of the predicted number of dead trees per cell
389 over the observed number (Gabry et al. 2019). For the posterior predictive checks, we used 50 random
390 samples from the model fit to generate 50 density curves and ensured curves were centered on the observed
391 distribution, paying special attention to model performance at capturing counts of zero.

392 Software and data availability

393 All data are available via the Open Science Framework. Statistical analyses were performed using the `brms`
394 packages. With the exception of the SfM software (Pix4Dmapper Cloud) and the GIS software QGIS, all
395 data carpentry and analyses were performed using R (R Core Team 2018).

396 Results

397 Tree detection algorithm performance

398 We found that the experimental `lmfx` algorithm with parameter values of `dist2d = 1` and `ws = 2.5` (Roussel
399 et al. 2019) performed the best across 7 measures of forest structure as measured by Pearson's correlation
400 with ground data (Table 2).

Table 2: Correlation and differences between the best performing tree detection algorithm (`lmfx` with `dist2d = 1` and `ws = 2.5`) and the ground data. An asterisk next to the correlation or RMSE indicates that this value was within 5% of the value of the best-performing algorithm/parameter set. Ground mean represents the mean value of the forest metric across the 110 field plots that were visible from the sUAS-derived imagery. The median error is calculated as the median of the differences between the air and ground values for the 110 visible plots. Thus, a positive number indicates an overestimate by the sUAS workflow and a negative number indicates an underestimate.

Forest structure metric	Ground mean	Correlation with ground	RMSE	Median error
total tree count	19	0.67*	8.68*	2
count of trees > 15 m	9.9	0.43	7.38	0
distance to 1st neighbor (m)	2.8	0.55*	1.16*	0.26

Forest structure metric	Ground mean	Correlation with ground	RMSE	Median error
distance to 2nd neighbor (m)	4.3	0.61*	1.70*	0.12
height (m); 25 th percentile	12	0.16	8.46	-1.2
height (m); mean	18	0.29	7.81*	-2.3
height (m); 75 th percentile	25	0.35	10.33*	-4

401 **Classification accuracy for live/dead and host/non-host**

402 The accuracy of live/dead classification on a withheld test dataset was 96.4%. The accuracy of species
 403 classification on a withheld testing dataset was 64.1%. The accuracy of WPB host/non-WPB-host (i.e.,
 404 ponderosa pine versus other tree species) on a withheld testing dataset was 71.8%.

405 **Site summary based on best tree detection algorithm and classification**

406 Across all study sites, we detected, segmented, and classified 452,413 trees. Of these trees, we classified
 407 118,879 as dead (26.3% mortality). Estimated site-level tree mortality ranged from 6.8% to 53.6%. See
 408 Supplemental Information for site summaries and comparisons to site-level mortality measured from field
 409 data.

410 **Effect of local structure and regional climate on tree mortality attributed to western pine
 411 beetle**

412 We detected a positive main effect of CWD on the probability of ponderosa pine mortality within each 20 x
 413 20-m cell (Figure 4). We found a positive main effect of proportion of host trees per cell (effect size: 0.76;
 414 95% CI: [0.70, 0.82]), with a greater proportion of host trees (i.e., ponderosa pine) in a cell increasing the
 415 probability of ponderosa pine mortality. We detected no effect of overall tree density nor overall basal area
 416 (i.e., including both ponderosa pine and non-host species; tree density effect size: -0.05; 95% CI: [-0.13, 0.03];
 417 basal area effect size: 0.00; 95% CI: [-0.11, 0.11]).

418 We found a positive two-way interaction between the overall tree density per cell and the proportion of trees
 419 that were hosts, which is equivalent to a positive effect of the density of host trees (effect size: 0.08; 95% CI:
 420 [0.03, 0.13]; Figure 4).

421 We found a negative effect of mean height of ponderosa pine on the probability of ponderosa mortality,
 422 suggesting that WPB attacked smaller trees, on average (effect size: -0.40; 95% CI: [-0.50, -0.30]). However,
 423 there was a positive interaction between CWD and ponderosa pine mean height, such that larger trees were

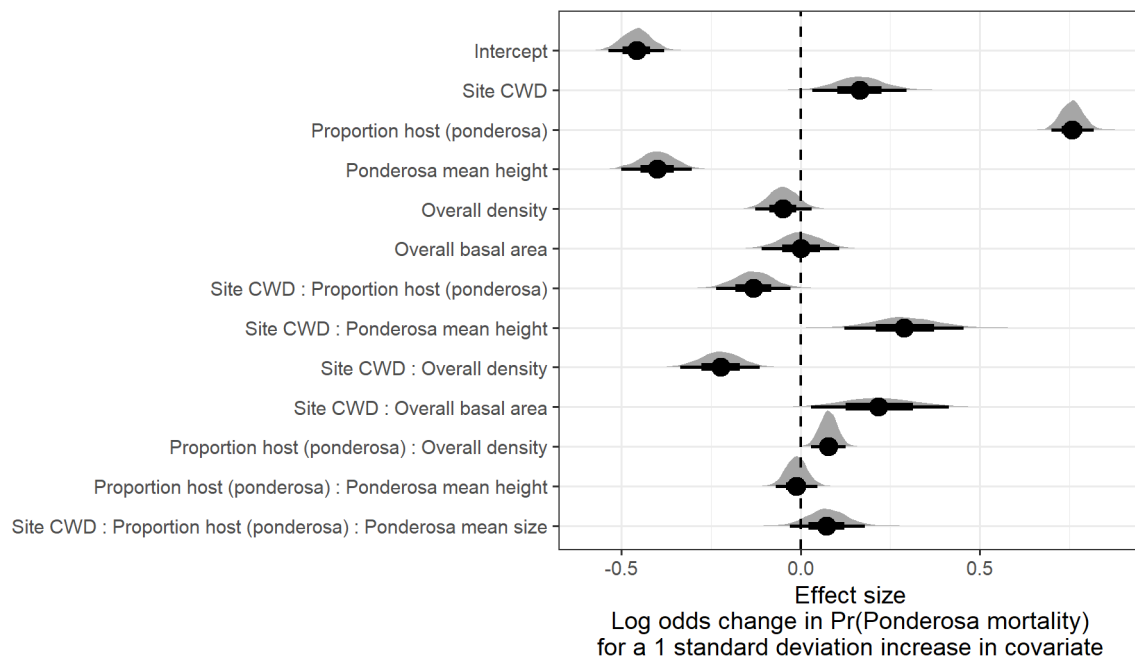


Figure 4: Posterior distributions of effect size from zero-inflated binomial model predicting the probability of ponderosa pine mortality in a 20 x 20-m cell given forest structure characteristics and site-level climatic water deficit (CWD). The gray filled area for each model covariate represents the probability density of the posterior distribution, the point underneath each density curve represents the median of the estimate, the bold interval surrounding the point estimate represents the 66% credible interval, and the thin interval surrounding the point estimate represents the 95% credible interval.

424 more likely to increase the local probability of ponderosa mortality in hotter, drier sites (effect size: 0.29;
425 95% CI: [0.12, 0.46]; Figure 5).

426 We found weakly negative effects of the site-level CWD interactions with both the proportion of host trees
427 and overall tree density (CWD/proportion host interaction effect size: -0.13; 95% CI: [-0.23, -0.03]; Figure 4;
428 CWD/overall tree density interaction effect size: -0.22; 95% CI: [-0.34, -0.11]; Figure 4; Figure 5). We found
429 a positive effect of the interaction between CWD and total basal area (effect size: 0.22; 95% CI: [0.03, 0.42];
430 Figure 4; Figure 5).

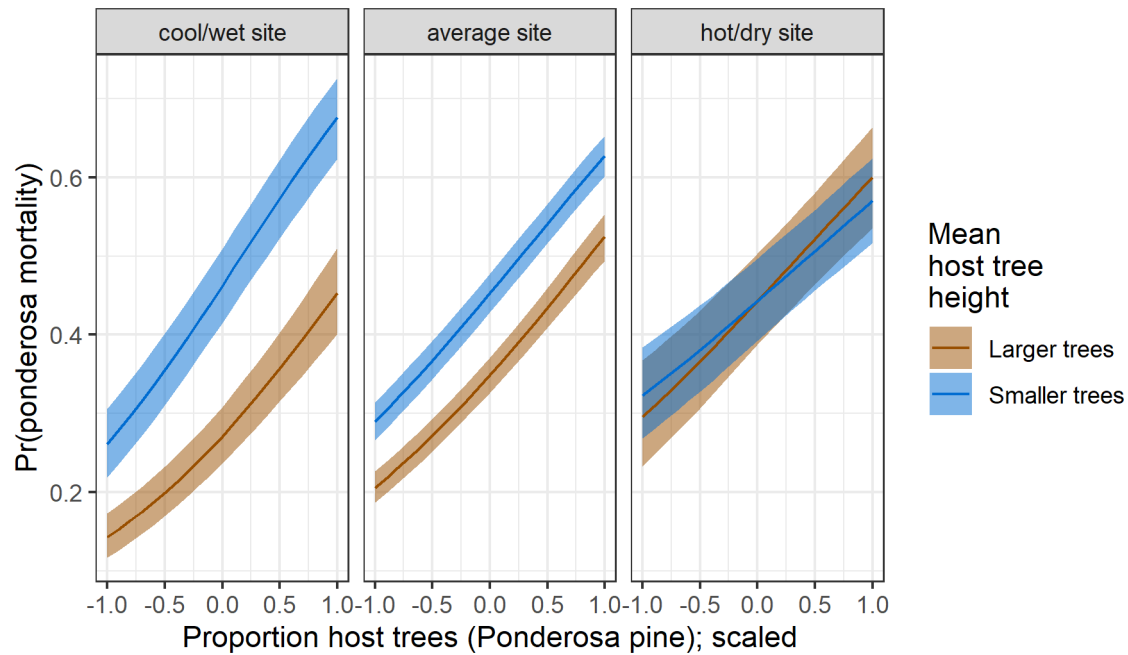


Figure 5: Line version of model results with 95% credible intervals showing primary influence of ponderosa pine structure on the probability of ponderosa pine mortality, and the interaction across climatic water deficit. The 'larger trees' line represents the mean height of ponderosa pine 0.7 standard deviations above the mean (approximately 24.1 m), and the 'smaller trees' line represents the mean height of ponderosa pine 0.7 standard deviations below the mean (approximately 12.1 m).

431 Discussion

432 This study represents a novel use of drones to further our understanding of the simultaneous effects of
433 local forest structure and composition with broad-scale environmental gradients on tree mortality attributed
434 to WPB. We found strong positive effects (effect sizes >0.4) of both the proportion of host trees and the
435 interaction between site CWD and host tree mean size (height) on the probability of ponderosa pine mortality.
436 Conversely, we found a strong negative effect (effect size <-0.4) of mean height of ponderosa pine. Site-level
437 CWD exerted a positive, but relatively weak, main effect on the probability of ponderosa mortality (effect

438 size: 0.16; 95% CI: [0.03, 0.30]). To that end, we did not measure tree water stress at an individual tree
439 level as in other recent work (Stephenson et al. 2019), and instead treated CWD as a general indicator of
440 tree stress following results of coarser-scale studies (e.g., Young et al. 2017), which may have contributed to
441 our failure to detect a stronger CWD effect. Also, our entire study area experienced the same extreme hot
442 drought between 2012 and 2015 and the variation of mortality explained by a main effect of CWD may be
443 dampened when most trees are experiencing a high degree of water stress (Floyd et al. 2009, Fettig et al.
444 2019).

445 Positive effect of host density and a negative effect of overall density

446 A number of mechanisms associated with the relative abundance of species in a local area might underlie the
447 strong effect of host proportion on the probability of host tree mortality. Frequency-dependent herbivory—
448 whereby mixed-species forests experience less herbivory compared to monocultures (as an extreme example)—
449 is common, especially for oligophagous insect species (Jactel and Brockerhoff 2007). Furthermore, it has been
450 demonstrated that nonhost volatiles reduce attraction of several species of bark beetles to their aggregation
451 pheromones (Seybold et al. 2018), including WPB (Fettig et al. 2005). To that end, combinations of nonhost
452 volatiles and an antiaggregation pheromone have been used successfully to reduce levels of tree mortality
453 attributed to WPB (e.g., Fettig et al. 2012). In general, Hayes et al. (2009) and Fettig et al. (2019) found
454 that measures of host availability explained less variation in mortality than measures of overall tree density,
455 but those conclusions were based on a response variable of “total number of dead host trees,” rather than
456 the number of dead host trees conditional on the total number of host trees as in our study (i.e., a binomial
457 response).

458 The negative relationship between overall tree density and the probability of ponderosa pine mortality
459 corroborates findings of coincident ground plots (Fettig et al. 2019, in their analysis using proportion of
460 trees killed as a response) and other work during the same hot drought (Restaino et al. 2019). The forest
461 structure (in the absence of management) is itself a product of climate and, with increasing importance at
462 finer spatial scales, topographic conditions (Fricker et al. 2019). Thus, the denser forest patches in our study
463 may indicate greater local water availability, more favorable conditions for tree growth and survivorship,
464 and increased resistance to beetle-induced mortality (Ma et al. 2010, Restaino et al. 2019, Fricker et al.
465 2019). The negative two-way interaction between site CWD and overall density that amplifies the negative
466 overall density effect in hotter, drier sites (effect size: -0.22; 95% CI: [-0.34, -0.11]) supports this explanation
467 if greater local tree density implies especially favorable growing conditions (and locally resistant trees) when
468 denser patches are found in hot, dry sites.

469 The positive relationship between host density and susceptibility to colonization by bark beetles has been so
470 well-documented at the experimental plot level (e.g., Raffa and Berryman 1987, Oliver 1995) that lowering
471 stand densities through selective harvest of hosts is commonly recommended for reducing future levels of tree
472 mortality attributed to bark beetles (Fettig and Hilszczański 2015), including WPB (Fettig 2016). Greater
473 host density shortens the flight distance required for WPB to disperse to new hosts, which likely facilitates
474 bark beetle spread, however we calibrated our aerial tree detection to ~400 m² areas rather than to individual
475 tree locations, so our data are insufficient to address these relationships. Increased density of ponderosa pine,
476 specifically, may disproportionately increase the competitive environment for host trees (and thus increase
477 their susceptibility to WPB colonization) if intraspecific competition amongst ponderosa pine trees is stronger
478 than interspecific competition as would be predicted with coexistence theory (Chesson 2000). Finally, greater
479 host densities increase the frequency that searching WPB land on hosts, rather than nonhosts, thus reducing
480 the amount of energy expended during host finding and selection as well as the time that searching WPB
481 spend exposed to predators.

482 **Positive interaction effect of CWD and basal area**

483 While overall tree density is likely an indicator of favorable microsite in fire-suppressed forests, overall basal
484 area is a better indicator of the local competitive environment especially in water-limited forests (Ma et al.
485 2010, Fricker et al. 2019). While we found no main effect of overall basal area on the probability of ponderosa
486 mortality, we did detect a clear interaction between site-level CWD and basal area such that mortality rates
487 of ponderosa pine in hotter, drier sites were greater when local overall basal area was high. This is a similar
488 interaction as found by Young et al. (2017), and we perhaps did not detect a similar main effect of basal
489 area as Young et al. (2017) because we partitioned this overall effect into the influence of finer-scale forest
490 structure and composition (e.g., number of host trees).

491 **Negative main effect of host tree mean size, but strong positive interaction with site CWD**

492 The negative main effect of host tree mean size was surprising, and appears to contradict long-standing
493 wisdom on the dynamics of western pine beetle in the Sierra Nevada. WPB exhibit a preference for trees 50.8
494 to 76.2 cm in diameter at breast height (Person 1928, 1931), and a positive relationship between host tree
495 size and levels of tree mortality attributed to WPB was reported by Fettig et al. (2019) in the coincident field
496 plots as well as in other recent studies (Restaino et al. 2019, Stephenson et al. 2019, Pile et al. 2019). Indeed,
497 Fettig et al. (2019) reported no mortality in ponderosa pine trees <10.0 cm DBH attributable to WPB and
498 found no tree size/mortality relationship for incense cedar or white fir in the coincident field plots. These
499 species represent 22.3% of the total tree mortality observed in their study, yet in our study all dead trees

500 were classified as ponderosa pine (see Methods) which could dampen positive effect of tree size on mortality.
501 Larger trees are more nutritious and are therefore ideal targets if local bark beetle density is high enough
502 to successfully initiate mass attack as can occur when many trees are under severe water stress (Bentz et
503 al. 2010, Boone et al. 2011, Kolb et al. 2016). In the recent hot drought, we expected that most trees
504 would be under severe water stress, setting the stage for increasing beetle density, successful mass attacks,
505 and targeting of larger trees. A possible explanation for our finding counter to this expectation is that our
506 observations represent the cumulative mortality of trees during a multi-year drought event and its aftermath.
507 Lower host tree mean size led to a greater probability of host mortality earlier in this drought (Pile et al.
508 2019, Stovall et al. 2019) and that signal might have persisted even as mortality continued to accumulate
509 driven by other factors. Another explanation may be that our extensive sampling design better captured
510 the contagious process by which bark beetles colonize smaller, suboptimal trees in the vicinity of the larger,
511 more desirable trees that are the focus of initial attack (Klein et al. 1978). If larger, desirable trees tend to
512 be associated with a greater local density of smaller trees that are also colonized in this contagious process,
513 then we might observe a negative relationship between tree size and ponderosa mortality rates. Finally, tree
514 growth rates may be a better predictor of susceptibility to WPB colonization than tree size per se, with
515 slower-growing trees being most vulnerable (Miller and Keen 1960). While slow-growing trees are often also
516 the largest trees, this may not be the case for our study sites especially given the legacy of fire exclusion
517 in the Sierra Nevada and its effect of perturbing forest structure far outside its natural range of variation
518 (Safford and Stevens 2017).

519 In hot, dry sites, larger average host size increased the probability of host mortality while smaller host sizes
520 increased the probability of host mortality in cooler, wetter sites. Notably, a similar pattern was shown
521 by Stovall et al. (2019) with a strong positive tree height/mortality relationship in areas with the greatest
522 vapor pressure deficit and no tree height/mortality relationship in areas with the lowest vapor pressure
523 deficit. Stovall et al. (2019) did not observe that this environmental dependence extended to a negative tree
524 height/mortality relationship (as we did) even at the lowest extremes of their vapor pressure deficit gradient,
525 perhaps because their entire study took place in the southern Sierra Nevada which represents a hotter, drier
526 portion of the more spatially extensive results we present here. Our work suggests that the WPB was cueing
527 into different aspects of forest structure across an environmental gradient in a spatial context in a parallel
528 manner to the temporal context noted by Stovall et al. (2019) and Pile et al. (2019), who observed that
529 mortality was increasingly driven by larger trees as the hot drought proceeded and became more severe.

530 All of our sites were considered in an “epidemic” population phase for WPB (>5 trees killed per hectare; see
531 Supplemental Information; Miller and Keen 1960, Hayes et al. 2009), but our results challenge the notion that

532 outbreak behavior by the WPB and subsequent tree mortality is always driven by greater tree size. Despite a
533 strong tree size/mortality relationship in coincident ground plots across our study area (Fettig et al. 2019),
534 our results from surveying the broader context surrounding those ground plots reveals different effects of
535 host tree size depending on CWD. Thus, it is possible that the massive tree mortality in hotter/drier Sierra
536 Nevada forests (lower latitudes and elevations; Asner et al. 2016, Young et al. 2017) during the 2012 to
537 2015 hot drought arose as a synergistic alignment of environmental conditions and local forest structure that
538 allowed WPB to successfully colonize large trees, rapidly increase in population size, and expand. It follows
539 that the unexpectedly low mortality in cooler/wetter Sierra Nevada forests compared to model predictions
540 based on coarser-scale forest structure data (Young et al. 2017) could be explained by a different WPB
541 response to local forest structure due to a lack of an alignment with favorable climate conditions.

542 **Limitations and future directions**

543 We have demonstrated that drones can be effective means of collecting forest data at multiple, vastly different
544 spatial scales to investigate a single, multi-scale phenomenon– from meters in between trees, to hundreds
545 of meters of elevation, to hundreds of thousands of meters of latitude. Some limitations remain but can be
546 overcome with further refinements in the use of this tool for forest ecology. Most of these limitations arise
547 from tree detection and classification uncertainty, and thus it was imperative to work with field data for
548 calibration and uncertainty reporting.

549 The greatest limitation in our study arising from classification uncertainty is in the assumption that all dead
550 trees were ponderosa pine, which we estimate from coincident field plots is true approximately 73.4% of
551 the time. Because the forest structure factors influencing the likelihood of individual tree mortality during
552 the hot drought depended on tree species (Stephenson et al. 2019), we cannot rule out that some of the
553 ponderosa pine mortality relationships to forest structure that we observed may be partially explained by
554 those relationships in other species that were misclassified as ponderosa pine using our methods. However,
555 the overall community composition across our study area was similar (Fettig et al. 2019) and we are able to
556 reproduce similar forest structure/mortality patterns in drone-derived data when restricting the scope of
557 analysis to only trees detected in the footprints of the coincident field plots, but with dramatically different
558 patterns observed when including data from the forest surrounding the coincident field plots (see Supplemental
559 information). Thus, we remain confident that the patterns we observed were driven primarily by the dynamic
560 between WPB and ponderosa pine. While spectral information of foliage could help classify living trees to
561 species, the species of standing dead trees were not spectrally distinct. This challenge of classifying standing
562 dead trees to species implies that a conifer forest system with less bark beetle and tree host diversity, such

563 as mountain pine beetle outbreaks in monocultures of lodgepole pine in the Intermountain West, should be
564 particularly amenable to the methods presented here even with minimal further refinement because dead
565 trees will almost certainly belong to a single species and have succumbed to colonization by a single bark
566 beetle species.

567 Some uncertainty surrounded our ability to detect trees using the geometry of the dense point clouds derived
568 with SfM. The horizontal accuracy of the tree detection was better than the vertical accuracy, which may
569 result from a more significant error contribution by the field-based calculations of tree height compared to
570 tree position relative to plot center (Table 2). Both the horizontal and vertical accuracy would likely improve
571 with better SfM point clouds, which can be enhanced with greater overlap between images (Frey et al. 2018)
572 or with oblique (i.e., off-nadir) imagery (James and Robson 2014). Frey et al. (2018) found that 95% overlap
573 was preferable for generating dense point clouds in forested areas, and James and Robson (2014) reduced
574 dense point cloud errors using imagery taken at 30 degrees off-nadir. We only achieved 91.6% overlap with
575 the X3 RGB camera and 83.9% overlap with the multispectral camera, and all imagery was nadir-facing.
576 While our live/dead classification was fairly accurate (96.4% on a withheld dataset), our species classifier
577 would likely benefit from better crown segmentation because the pixel-level reflectance values within each
578 crown are averaged to characterize the “spectral signature” of each tree. With better delineation of each
579 tree crown, the mean value of pixels within each tree crown will likely be more representative of that tree’s
580 spectral signature. Better crown segmentation might most readily be achieved through greater overlap in
581 imagery. We anticipate that computer vision and deep learning will prove helpful in overcoming some of
582 these detection and classification challenges (Gray et al. 2019).

583 Another limitation of our study is in our use of the probability of ponderosa mortality as our key response
584 variable. This measure is well-suited to understanding the dynamics between WPB colonization behavior and
585 host tree susceptibility, but may not capture impacts on the forest ecosystem and its services as well as a
586 measure of biomass reduction such as tree basal area.

587 Conclusions

588 Climate change adaptation strategies emphasize management action that considers whole-ecosystem responses
589 to inevitable change (Millar et al. 2007), which requires a macroecological understanding of how phenomena at
590 multiple scales can interact. Tree vulnerability to environmental stressors presents only a partial explanation
591 for tree mortality patterns during hot droughts, especially when bark beetles are present. We’ve shown that
592 drones can be a valuable tool for investigating multi-scalar phenomena, such as how local forest structure
593 combines with environmental conditions to shape forest insect disturbance. Understanding the conditions

594 that drive dry western U.S. forest responses to disturbances such as bark beetle outbreaks will be vital for
595 predicting outcomes from increasing disturbance frequency and intensity exacerbated by climate change. Our
596 study suggests that outcomes will depend on interactions between local forest structure and broad-scale
597 environmental gradients, with the potential for cross-scale interactions to enhance our current understanding
598 of forest insect dynamics.

599 **References**

- 600 Anderegg, W. R. L., J. A. Hicke, R. A. Fisher, C. D. Allen, J. Aukema, B. Bentz, S. Hood, J. W. Lichstein,
601 A. K. Macalady, N. McDowell, Y. Pan, K. Raffa, A. Sala, J. D. Shaw, N. L. Stephenson, C. Tague, and
602 M. Zeppel. 2015. Tree mortality from drought, insects, and their interactions in a changing climate. *New*
603 *Phytologist* 208:674–683.
- 604 Asner, G. P., P. G. Brodrick, C. B. Anderson, N. Vaughn, D. E. Knapp, and R. E. Martin. 2016. Progressive
605 forest canopy water loss during the 2012–2015 California drought. *Proceedings of the National Academy of*
606 *Sciences* 113:E249–E255.
- 607 Baldwin, B. G., A. H. Thornhill, W. A. Freyman, D. D. Ackerly, M. M. Kling, N. Morueta-Holme, and B. D.
608 Mishler. 2017. Species richness and endemism in the native flora of California. *American Journal of Botany*
609 104:487–501.
- 610 Bedard, W. D., P. E. Tilden, D. L. Wood, R. M. Silverstein, R. G. Brownlee, and J. O. Rodin. 1969.
611 Western pine beetle: Field response to its sex pheromone and a synergistic host terpene, myrcene. *Science*
612 164:1284–1285.
- 613 Bentz, B. J., J. Régnière, C. J. Fettig, E. M. Hansen, J. L. Hayes, J. A. Hicke, R. G. Kelsey, J. F. Negrón,
614 and S. J. Seybold. 2010. Climate change and bark beetles of the western United States and Canada: Direct
615 and indirect effects. *BioScience* 60:602–613.
- 616 Berryman, A. A. 1982. Population dynamics of bark beetles. Pages 264–314 in *Bark Beetles in North*
617 *American Conifers: A System for the Study of Evolutionary Biology*.
- 618 Boone, C. K., B. H. Aukema, J. Bohlmann, A. L. Carroll, and K. F. Raffa. 2011. Efficacy of tree defense
619 physiology varies with bark beetle population density: A basis for positive feedback in eruptive species.
620 *Canadian Journal of Forest Research* 41:1174–1188.
- 621 Brodrick, P. G., and G. P. Asner. 2017. Remotely sensed predictors of conifer tree mortality during severe
622 drought. *Environmental Research Letters* 12:115013.
- 623 Brooks, S. P., and A. Gelman. 1998. General methods for monitoring convergence of iterative simulations.
624 *Journal of Computational and Graphical Statistics* 7:434.
- 625 Bürkner, P.-C. 2017. **brms**: An *R* package for bayesian multilevel models using *Stan*. *Journal of Statistical*
626 *Software* 80:1–28.
- 627 Byers, J. A., and D. L. Wood. 1980. Interspecific inhibition of the response of the bark beetles, *Dendroctonus*

- 628 *brevicomis* and *Ips paraconfusus*, to their pheromones in the field. Journal of Chemical Ecology 6:149–164.
- 629 Carpenter, B., A. Gelman, M. D. Hoffman, D. Lee, B. Goodrich, M. Betancourt, M. Brubaker, J. Guo, P. Li,
630 and A. Riddell. 2017. Stan: A Probabilistic Programming Language. Journal of Statistical Software 76:1–32.
- 631 Chesson, P. 2000. Mechanisms of maintenance of species diversity. Annual Review of Ecology and Systematics
632 31:343–366.
- 633 Chubaty, A. M., B. D. Roitberg, and C. Li. 2009. A dynamic host selection model for mountain pine beetle,
634 *Dendroctonus ponderosae* Hopkins. Ecological Modelling 220:1241–1250.
- 635 Clevers, J., and A. Gitelson. 2013. Remote estimation of crop and grass chlorophyll and nitrogen content using
636 red-edge bands on Sentinel-2 and -3. International Journal of Applied Earth Observation and Geoinformation
637 23:344–351.
- 638 Coops, N. C., M. Johnson, M. A. Wulder, and J. C. White. 2006. Assessment of QuickBird high spatial
639 resolution imagery to detect red attack damage due to mountain pine beetle infestation. Remote Sensing of
640 Environment 103:67–80.
- 641 DJI. 2015a. Zenmuse X3 - Creativity Unleashed. <https://www.dji.com/zenmuse-x3/info>.
- 642 DJI. 2015b. DJI - The World Leader in Camera Drones/Quadcopters for Aerial Photography. <https://www.dji.com/matrice100/info>.
- 644 DronesMadeEasy. 2018. Map Pilot for DJI on iOS. <https://itunes.apple.com/us/app/map-pilot-for-dji/id1014765000?mt=8>.
- 646 Evenden, M. L., C. M. Whitehouse, and J. Sykes. 2014. Factors influencing flight capacity of the mountain
647 pine beetle (Coleoptera: Curculionidae: Scolytinae). Environmental Entomology 43:187–196.
- 648 Eysn, L., M. Hollaus, E. Lindberg, F. Berger, J.-M. Monnet, M. Dalponte, M. Kobal, M. Pellegrini, E.
649 Lingua, D. Mongus, and N. Pfeifer. 2015. A benchmark of LiDAR-based single tree detection methods using
650 heterogeneous forest data from the alpine space. Forests 6:1721–1747.
- 651 Farr, T. G., P. A. Rosen, E. Caro, R. Crippen, R. Duren, S. Hensley, M. Kobrick, M. Paller, E. Rodriguez, L.
652 Roth, D. Seal, S. Shaffer, J. Shimada, J. Umland, M. Werner, M. Oskin, D. Burbank, and D. Alsdorf. 2007.
653 The shuttle radar topography mission. Reviews of Geophysics 45.
- 654 Fettig, C. J. 2012. Chapter 2: Forest health and bark beetles. *in* Managing Sierra Nevada Forests. PSW-
655 GTR-237. USDA Forest Service.

- 656 Fettig, C. J. 2016. Native bark beetles and wood borers in Mediterranean forests of California. Pages 499–528
657 in Insects and diseases of Mediterranean Forest systems. Springer International Publishing, Switzerland.
- 658 Fettig, C. J., and J. Hilszczański. 2015. Management strategies for bark beetles in conifer forests. Pages
659 555–584 in Bark Beetles. Elsevier.
- 660 Fettig, C. J., K. D. Klepzig, R. F. Billings, A. S. Munson, T. E. Nebeker, J. F. Negrón, and J. T. Nowak. 2007.
661 The effectiveness of vegetation management practices for prevention and control of bark beetle infestations in
662 coniferous forests of the western and southern United States. *Forest Ecology and Management* 238:24–53.
- 663 Fettig, C. J., S. R. McKelvey, C. P. Dabney, D. P. W. Huber, C. G. Lait, D. L. Fowler, and J. H. Borden. 2012.
664 Efficacy of “Verbenone Plus” for protecting ponderosa pine trees and stands from *Dendroctonus brevicomis*
665 (Coleoptera: Curculionidae) attack in British Columbia and California. *Journal of Economic Entomology*
666 105:1668–1680.
- 667 Fettig, C. J., S. R. McKelvey, and D. P. W. Huber. 2005. Nonhost angiosperm volatiles and Verbenone disrupt
668 response of western pine beetle, *Dendroctonus brevicomis* (Coleoptera: Scolytidae), to attractant-baited traps.
669 *Journal of Economic Entomology* 98:2041–2048.
- 670 Fettig, C. J., L. A. Mortenson, B. M. Bulaon, and P. B. Foulk. 2019. Tree mortality following drought in the
671 central and southern Sierra Nevada, California, U.S. *Forest Ecology and Management* 432:164–178.
- 672 Flint, L. E., A. L. Flint, J. H. Thorne, and R. Boynton. 2013. Fine-scale hydrologic modeling for regional land-
673 scape applications: The California Basin Characterization Model development and performance. *Ecological
674 Processes* 2:25.
- 675 Floyd, M. L., M. Clifford, N. S. Cobb, D. Hanna, R. Delph, P. Ford, and D. Turner. 2009. Relationship of
676 stand characteristics to drought-induced mortality in three Southwestern piñonJuniper woodlands. *Ecological
677 Applications* 19:1223–1230.
- 678 Franceschi, V. R., P. Krokene, E. Christiansen, and T. Krekling. 2005. Anatomical and chemical defenses of
679 conifer bark against bark beetles and other pests. *New Phytologist* 167:353–376.
- 680 Frey, J., K. Kovach, S. Stemmler, and B. Koch. 2018. UAV photogrammetry of forests as a vulnerable
681 process. A sensitivity analysis for a structure from motion RGB-image pipeline. *Remote Sensing* 10:912.
- 682 Fricker, G. A., N. W. Synes, J. M. Serra-Diaz, M. P. North, F. W. Davis, and J. Franklin. 2019. More than
683 climate? Predictors of tree canopy height vary with scale in complex terrain, Sierra Nevada, CA (USA).
684 *Forest Ecology and Management* 434:142–153.

- 685 Gabry, J., D. Simpson, A. Vehtari, M. Betancourt, and A. Gelman. 2019. Visualization in Bayesian workflow.
686 Journal of the Royal Statistical Society: Series A (Statistics in Society) 182:389–402.
- 687 Geiszler, D. R., and R. I. Gara. 1978. Mountain pine beetle attack dynamics in lodgepole pine. *in* Theory
688 and Practice of Mountain Pine Beetle Management in Lodgepole Pine Forests: Symposium Proceedings. A.
689 A. Berryman, G. D. Amman and R. W. Stark (Eds). Pullman, WA, USA.
- 690 Gitelson, A., and M. N. Merzlyak. 1994. Spectral reflectance changes associated with autumn senescence of
691 *Aesculus hippocastanum* L. And *Acer platanoides* L. Leaves. Spectral features and relation to chlorophyll
692 estimation. Journal of Plant Physiology 143:286–292.
- 693 Graf, M., M. Reid, B. Aukema, and B. Lindgren. 2012. Association of tree diameter with body size and lipid
694 content of mountain pine beetles. The Canadian Entomologist 144:467–477.
- 695 Gray, P. C., A. B. Fleishman, D. J. Klein, M. W. McKown, V. S. Bézy, K. J. Lohmann, and D. W. Johnston.
696 2019. A convolutional neural network for detecting sea turtles in drone imagery. Methods in Ecology and
697 Evolution 10:345–355.
- 698 Griffin, D., and K. J. Anchukaitis. 2014. How unusual is the 2012-2014 California drought? Geophysical
699 Research Letters 41:9017–9023.
- 700 Hayes, C. J., C. J. Fettig, and L. D. Merrill. 2009. Evaluation of multiple funnel traps and stand characteristics
701 for estimating western pine beetle-caused tree mortality. Journal of Economic Entomology 102:2170–2182.
- 702 Hijmans, R. J., J. van Etten, M. Sumner, J. Cheng, A. Bevan, R. Bivand, L. Busetto, M. Canty, D. Forrest,
703 A. Ghosh, D. Golicher, J. Gray, J. A. Greenberg, P. Hiemstra, I. for M. A. Geosciences, C. Karney, M.
704 Mattiuzzi, S. Mosher, J. Nowosad, E. Pebesma, O. P. Lamigueiro, E. B. Racine, B. Rowlingson, A. Shortridge,
705 B. Venables, and R. Wueest. 2019. Raster: Geographic data analysis and modeling.
- 706 Hoffman, M. D., and A. Gelman. 2014. The No-U-Turn Sampler: Adaptively setting path lengths in
707 Hamiltonian Monte Carlo. Journal of Machine Learning Research 15:31.
- 708 Hunziker, P. 2017. Velox: Fast raster manipulation and extraction.
- 709 Jactel, H., and E. G. Brockerhoff. 2007. Tree diversity reduces herbivory by forest insects. Ecology Letters
710 10:835–848.
- 711 Jakubowski, M. K., W. Li, Q. Guo, and M. Kelly. 2013. Delineating individual trees from LiDAR data: A
712 comparison of vector- and raster-based segmentation approaches. Remote Sensing 5:4163–4186.
- 713 James, M. R., and S. Robson. 2014. Mitigating systematic error in topographic models derived from UAV

- 714 and ground-based image networks. *Earth Surface Processes and Landforms* 39:1413–1420.
- 715 Jeronimo, S. M. A., V. R. Kane, D. J. Churchill, J. A. Lutz, M. P. North, G. P. Asner, and J. F. Franklin.
716 2019. Forest structure and pattern vary by climate and landform across active-fire landscapes in the montane
717 Sierra Nevada. *Forest Ecology and Management* 437:70–86.
- 718 Kaiser, K. E., B. L. McGlynn, and R. E. Emanuel. 2013. Ecohydrology of an outbreak: Mountain pine beetle
719 impacts trees in drier landscape positions first: ECOHYDROLOGY OF A MOUNTAIN PINE BEETLE
720 OUTBREAK. *Ecohydrology* 6:444–454.
- 721 Kane, V. R., M. P. North, J. A. Lutz, D. J. Churchill, S. L. Roberts, D. F. Smith, R. J. McGaughey, J. T.
722 Kane, and M. L. Brooks. 2014. Assessing fire effects on forest spatial structure using a fusion of Landsat and
723 airborne LiDAR data in Yosemite National Park. *Remote Sensing of Environment* 151:89–101.
- 724 Klein, W. H., D. L. Parker, and C. E. Jensen. 1978. Attack, emergence, and stand depletion trends of the
725 mountain pine beetle in a lodgepole pine stand during an outbreak. *Environmental Entomology* 7:732–737.
- 726 Kolb, T. E., C. J. Fettig, M. P. Ayres, B. J. Bentz, J. A. Hicke, R. Mathiasen, J. E. Stewart, and A. S. Weed.
727 2016. Observed and anticipated impacts of drought on forest insects and diseases in the United States. *Forest
728 Ecology and Management* 380:321–334.
- 729 Kuhn, M. 2008. Building predictive models in R using the caret package. *Journal of Statistical Software*
730 28:1–26.
- 731 Larson, A. J., and D. Churchill. 2012. Tree spatial patterns in fire-frequent forests of western North America,
732 including mechanisms of pattern formation and implications for designing fuel reduction and restoration
733 treatments. *Forest Ecology and Management* 267:74–92.
- 734 Li, W., Q. Guo, M. K. Jakubowski, and M. Kelly. 2012. A new method for segmenting individual trees from
735 the LiDAR point cloud. *Photogrammetric Engineering & Remote Sensing* 78:75–84.
- 736 Logan, J. A., P. White, B. J. Bentz, and J. A. Powell. 1998. Model analysis of spatial patterns in mountain
737 pine beetle outbreaks. *Theoretical Population Biology* 53:236–255.
- 738 Ma, S., A. Concilio, B. Oakley, M. North, and J. Chen. 2010. Spatial variability in microclimate in a
739 mixed-conifer forest before and after thinning and burning treatments. *Forest Ecology and Management*.
740 259: 904–915 259:904–915.
- 741 Meyer, F., and S. Beucher. 1990. Morphological segmentation. *Journal of Visual Communication and Image
742 Representation* 1:21–46.

- 743 Micasense. 2015. MicaSense. <https://support.micasense.com/hc/en-us/articles/215261448-RedEdge-User->
- 744 Manual-PDF-Download-.
- 745 Millar, C. I., N. L. Stephenson, and S. L. Stephens. 2007. Climate change and forests of the future: Managing
746 in the face of uncertainty. *Ecological Applications* 17:2145–2151.
- 747 Millar, C. I., R. D. Westfall, D. L. Delany, M. J. Bokach, A. L. Flint, and L. E. Flint. 2012. Forest mortality in
748 high-elevation whitebark pine (*Pinus albicaulis*) forests of eastern California, USA: Influence of environmental
749 context, bark beetles, climatic water deficit, and warming. *Canadian Journal of Forest Research* 42:749–765.
- 750 Miller, J. M., and F. P. Keen. 1960. Biology and control of the western pine beetle: A summary of the first
751 fifty years of research. US Department of Agriculture.
- 752 Mitchell, R. G., and H. K. Preisler. 1991. Analysis of spatial patterns of lodgepole pine attacked by outbreak
753 populations of the mountain pine beetle. *Forest Science* 37:1390–1408.
- 754 Moeck, H. A., D. L. Wood, and K. Q. Lindahl. 1981. Host selection behavior of bark beetles (Coleoptera:
755 Scolytidae) attacking *Pinus ponderosa*, with special emphasis on the western pine beetle, *Dendroctonus*
756 *brevicomis*. *Journal of Chemical Ecology* 7:49–83.
- 757 Morris, J. L., S. Cottrell, C. J. Fettig, W. D. Hansen, R. L. Sherriff, V. A. Carter, J. L. Clear, J. Clement, R.
758 J. DeRose, J. A. Hicke, P. E. Higuera, K. M. Mattor, A. W. R. Seddon, H. T. Seppä, J. D. Stednick, and S.
759 J. Seybold. 2017. Managing bark beetle impacts on ecosystems and society: Priority questions to motivate
760 future research. *Journal of Applied Ecology* 54:750–760.
- 761 Oliver, W. W. 1995. Is self-thinning in ponderosa pine ruled by *Dendroctonus* bark beetles? Page 6 *in* Forest
762 health through silviculture: Proceedings of the 1995 National Silviculture Workshop.
- 763 Pau, G., F. Fuchs, O. Sklyar, M. Boutros, and W. Huber. 2010. EBImage: An R package for image processing
764 with applications to cellular phenotypes. *Bioinformatics* 26:979–981.
- 765 Person, H. L. 1928. Tree selection by the western pine beetle. *Journal of Forestry* 26:564–578.
- 766 Person, H. L. 1931. Theory in explanation of the selection of certain trees by the western pine beetle. *Journal*
767 *of Forestry* 29:696–699.
- 768 Pile, L. S., M. D. Meyer, R. Rojas, O. Roe, and M. T. Smith. 2019. Drought impacts and compounding
769 mortality on forest trees in the southern Sierra Nevada. *Forests* 10:237.
- 770 Plowright, A. 2018. ForestTools: Analyzing remotely sensed forest data.
- 771 Preisler, H. K. 1993. Modelling Spatial Patterns of Trees Attacked by Bark-Beetles. *Applied Statistics* 42:501.

- 772 Raffa, K. F., B. H. Aukema, B. J. Bentz, A. L. Carroll, J. A. Hicke, M. G. Turner, and W. H. Romme. 2008.
- 773 Cross-scale drivers of natural disturbances prone to anthropogenic amplification: The dynamics of bark beetle
- 774 eruptions. *BioScience* 58:501–517.
- 775 Raffa, K. F., and A. A. Berryman. 1983. The role of host plant resistance in the colonization behavior and
- 776 ecology of bark beetles (Coleoptera: Scolytidae). *Ecological Monographs* 53:27–49.
- 777 Raffa, K. F., and A. A. Berryman. 1987. Interacting selective pressures in conifer-bark beetle systems: A
- 778 basis for reciprocal adaptations? *The American Naturalist* 129:234–262.
- 779 Raffa, K. F., J.-C. Grégoire, and B. Staffan Lindgren. 2015. Natural history and ecology of bark beetles.
- 780 Pages 1–40 in *Bark Beetles*. Elsevier.
- 781 R Core Team. 2018. R: A language and environment for statistical computing. R Foundation for Statistical
- 782 Computing, Vienna, Austria.
- 783 Restaino, C., D. Young, B. Estes, S. Gross, A. Wuenschel, M. Meyer, and H. Safford. 2019. Forest
- 784 structure and climate mediate drought-induced tree mortality in forests of the Sierra Nevada, USA. *Ecological*
- 785 *Applications* 0:e01902.
- 786 Robeson, S. M. 2015. Revisiting the recent California drought as an extreme value. *Geophysical Research*
- 787 *Letters* 42:6771–6779.
- 788 Rouse, W., R. H. Haas, W. Deering, and J. A. Schell. 1973. Monitoring the vernal advancement and
- 789 retrogradation (green wave effect) of natural vegetation. Type II Report, Goddard Space Flight Center,
- 790 Greenbelt, MD, USA.
- 791 Roussel, J.-R. 2019. lidRplugins: Extra functions and algorithms for lidR package.
- 792 Roussel, J.-R., D. Auty, F. De Boissieu, and A. S. Meador. 2019. lidR: Airborne LiDAR data manipulation
- 793 and visualization for forestry applications.
- 794 Safford, H. D., and J. T. Stevens. 2017. Natural range of variation for yellow pine and mixed-conifer forests
- 795 in the Sierra Nevada, Southern Cascades, and Modoc and Inyo National Forests, California, USA. Page 241.
- 796 dos Santos, A. A., J. Marcato Junior, M. S. Araújo, D. R. Di Martini, E. C. Tetila, H. L. Siqueira, C. Aoki, A.
- 797 Eltner, E. T. Matsubara, H. Pistori, R. Q. Feitosa, V. Liesenberg, and W. N. Gonçalves. 2019. Assessment of
- 798 CNN-Based Methods for Individual Tree Detection on Images Captured by RGB Cameras Attached to UAVs.
- 799 Sensors (Basel, Switzerland) 19.
- 800 Seidl, R., J. Müller, T. Hothorn, C. Bässler, M. Heurich, and M. Kautz. 2016. Small beetle, large-scale

- 801 drivers: How regional and landscape factors affect outbreaks of the European spruce bark beetle. *The Journal*
802 of applied ecology
- 803 Senf, C., E. M. Campbell, D. Pflugmacher, M. A. Wulder, and P. Hostert. 2017. A multi-scale analysis of
804 western spruce budworm outbreak dynamics. *Landscape Ecology* 32:501–514.
- 805 Seybold, S. J., B. J. Bentz, C. J. Fettig, J. E. Lundquist, R. A. Progar, and N. E. Gillette. 2018. Management
806 of western North American bark beetles with semiochemicals. *Annual Review of Entomology* 63:407–432.
- 807 Shepherd, W. P., D. P. W. Huber, S. J. Seybold, and C. J. Fettig. 2007. Antennal responses of the western
808 pine beetle, *Dendroctonus brevicomis* (Coleoptera: Curculionidae), to stem volatiles of its primary host,
809 *Pinus ponderosa*, and nine sympatric nonhost angiosperms and conifers. *Chemoecology* 17:209–221.
- 810 Shiklomanov, A. N., B. A. Bradley, K. M. Dahlin, A. M. Fox, C. M. Gough, F. M. Hoffman, E. M. Middleton,
811 S. P. Serbin, L. Smallman, and W. K. Smith. 2019. Enhancing global change experiments through integration
812 of remote-sensing techniques. *Frontiers in Ecology and the Environment* 0.
- 813 Shin, P., T. Sankey, M. Moore, and A. Thode. 2018. Evaluating unmanned aerial vehicle images for estimating
814 forest canopy fuels in a ponderosa pine stand. *Remote Sensing* 10:1266.
- 815 Stephenson, N. 1998. Actual evapotranspiration and deficit: Biologically meaningful correlates of vegetation
816 distribution across spatial scales. *Journal of Biogeography* 25:855–870.
- 817 Stephenson, N. L., A. J. Das, N. J. Ampersee, and B. M. Bulaon. 2019. Which trees die during drought?
818 The key role of insect host-tree selection. *Journal of Ecology*:75.
- 819 Stovall, A. E. L., H. Shugart, and X. Yang. 2019. Tree height explains mortality risk during an intense
820 drought. *Nature Communications* 10:1–6.
- 821 Thistle, H. W., H. Peterson, G. Allwine, B. Lamb, T. Strand, E. H. Holsten, and P. J. Shea. 2004. Surrogate
822 pheromone plumes in three forest trunk spaces: Composite statistics and case studies. *Forest Science* 50.
- 823 USDAFS. 2017, December 12. Press Release: Record 129 million dead trees in California.
- 824 USDAFS. 2019, February 11. Press Release: Survey finds 18 million trees died in California in 2018.
825 https://www.fs.usda.gov/Internet/FSE_DOCUMENTS/FSEPRD609321.pdf.
- 826 Vega, C., A. Hamrouni, S. El Mokhtari, J. Morel, J. Bock, J. P. Renaud, M. Bouvier, and S. Durrieu. 2014.
827 PTrees: A point-based approach to forest tree extraction from LiDAR data. *International Journal of Applied
828 Earth Observation and Geoinformation* 33:98–108.

- 829 Wallin, K. F., and K. F. Raffa. 2004. Feedback between Individual Host Selection Behavior and Population
830 Dynamics in an Eruptive Herbivore. *Ecological Monographs* 74:101–116.
- 831 Waring, R. H., and G. B. Pitman. 1985. Modifying Lodgepole Pine Stands to Change Susceptibility to
832 Mountain Pine Beetle Attack. *Ecology* 66:889–897.
- 833 Weinstein, B. G., S. Marconi, S. Bohlman, A. Zare, and E. White. 2019. Individual Tree-Crown Detection in
834 RGB Imagery Using Semi-Supervised Deep Learning Neural Networks. *Remote Sensing* 11:1309.
- 835 Wyngaard, J., L. Barbieri, A. Thomer, J. Adams, D. Sullivan, C. Crosby, C. Parr, J. Klump, S. Raj Shrestha,
836 and T. Bell. 2019. Emergent challenges for science sUAS data management: Fairness through community
837 engagement and best practices development. *Remote Sensing* 11:1797.
- 838 Young, D. J. N., J. T. Stevens, J. M. Earles, J. Moore, A. Ellis, A. L. Jirka, and A. M. Latimer. 2017.
839 Long-term climate and competition explain forest mortality patterns under extreme drought. *Ecology Letters*
840 20:78–86.
- 841 Zhang, W., J. Qi, P. Wan, H. Wang, D. Xie, X. Wang, and G. Yan. 2016. An easy-to-use airborne LiDAR
842 data filtering method based on cloth simulation. *Remote Sensing* 8:501.